Dissociative photoionization of methyl chloride studied with threshold photoelectron-photoion coincidence velocity imaging

Xiaofeng Tang, Xiaoguo Zhou, Manman Wu, Shilin Liu, Fuyi Liu et al.

Citation: J. Chem. Phys. **136**, 034304 (2012); doi: 10.1063/1.3676411
View online: http://dx.doi.org/10.1063/1.3676411
View Table of Contents: http://jcp.aip.org/resource/1/JCPSA6/v136/i3
Published by the American Institute of Physics.

Dissociative photoionization of methyl chloride studied with threshold photoelectron-photoion coincidence velocity imaging

Xiaofeng Tang,[1,2] Xiaoguo Zhou,[1,a)] Manman Wu,[1] Shilin Liu,[1] Fuyi Liu,[2] Xiaobin Shan,[2] and Liusi Sheng[2]

[1]*Hefei National Laboratory for Physical Sciences at the Microscale and Department of Chemical Physics, University of Science and Technology of China, Hefei, Anhui 230026, China*

[2]*National Synchrotron Radiation Laboratory, University of Science and Technology of China, Hefei, Anhui 230029, China*

(Received 4 November 2011; accepted 22 December 2011; published online 17 January 2012)

Utilizing threshold photoelectron-photoion coincidence (TPEPICO) velocity imaging, dissociation of state-selected CH_3Cl^+ ions was investigated in the excitation energy range of 11.0–18.5 eV. TPEPICO time-of-flight mass spectra and three-dimensional time-sliced velocity images of CH_3^+ dissociated from $CH_3Cl^+(A^2A_1$ and $B^2E)$ ions were recorded. CH_3^+ was kept as the most dominant fragment ion in the present energy range, while the branching ratio of CH_2Cl^+ fragment was very low. For dissociation of $CH_3Cl^+(A^2A_1)$ ions, a series of homocentric rings was clearly observed in the CH_3^+ image, which was assigned as the excitation of umbrella vibration of CH_3^+ ions. Moreover, a dependence of anisotropic parameters on the vibrational states of $CH_3^+(1^1A')$ provided a direct experimental evidence of a shallow potential well along the C–Cl bond rupture. For $CH_3Cl^+(B^2E)$ ions, total kinetic energy released distribution for CH_3^+ fragmentation showed a near Maxwell-Boltzmann profile, indicating that the Cl-loss pathway from the B^2E state was statistical predissociation. With the aid of calculated Cl-loss potential energy curves of CH_3Cl^+, CH_3^+ formation from $CH_3Cl^+(A^2A_1)$ ions was a rapid direct fragmentation, while $CH_3Cl^+(B^2E)$ ions statistically dissociated to $CH_3^+ + Cl$ via internal conversion to the high vibrational states of X^2E. © *2012 American Institute of Physics*. [doi:10.1063/1.3676411]

I. INTRODUCTION

As an important chemical reagent with a high symmetry of C_{3V}, spectroscopy and molecular structures of methyl chloride (CH_3Cl), and its ion have been widely studied in the past decades. The electron configuration of the ground state of CH_3Cl molecule is $(1a_1)^2(2a_1)^2(1e)^4(3a_1)^2(2e)^4$, X^1A_1.[1–3] Removing an electron from outer orbitals, e.g., 2e, $3a_1$, or 1e, can generate CH_3Cl^+ ion in the X^2E, A^2A_1, or B^2E states, respectively. An early high resolution photoelectron spectrum of CH_3Cl in the excitation energy range of 11–20 eV was recorded using He I ionization source,[3] where the lower lying electronic states of CH_3Cl^+ were assigned. Vibrational structure was observed for the X^2E ground ionic state, while the A^2A_1 and B^2E states of CH_3Cl^+ ions overlapped without any vibrational structure. Vertical ionization energies for the $X^2E_{3/2}$ ($^2E_{1/2}$), A^2A_1, and $B^2E_{3/2}$ ($^2E_{1/2}$) ionic states were measured to be 11.289 (11.316), 14.4, and 15.4 (16.0) eV, respectively. Using synchrotron radiation (SR) as light source, Olney *et al.*[2] and Locht *et al.*[4] measured absorption spectrum and threshold photoelectron spectrum (TPES) of CH_3Cl. Angular distributions of electron in photoionization of CH_3Cl were measured as well, and their anisotropic parameters were obtained.[5–7]

Combining electron impact ionization and time-of-flight (TOF) mass spectrometer, Tsuda *et al.*[8,9] recorded the ionization efficiency curves of CH_3^+, CH_2Cl^+, and CH_2^+ fragment ions and obtained their appearance potentials (AP). By improving the energy resolution of electron, Lossing[10] and Werner *et al.*[11] observed ionization efficiency curves of CH_2Cl^+ and CH_3^+, and suggested their adiabatic appearance potentials at 13.02 eV for CH_2Cl^+ and 13.38 eV for CH_3^+. Subsequently, Brunetti *et al.* measured the cross section and branching ratios of CH_2Cl^+ and CH_3^+ fragment ions using penning ionization,[12,13] where CH_2Cl^+ fragment ions appeared at adiabatic onset (13.02 eV) with a low branching ratio. However, CH_2Cl^+ was not observed at the excitation energy of lower than 15 eV in photoelectron-photoion coincidence (PEPICO) experiments,[14,15] although the energy was higher than its AP(CH_2Cl^+, 13.02 eV). A similar phenomenon was also obtained in the photofragmentation of CH_3Cl^+ at 366 nm, where CH_3Cl^+ ions were produced by 13.5 eV electron impact.[16] Thus a potential explanation for this inconsistency is needed.

For the dissociation dynamics of state-selected CH_3Cl^+ ions, several experimental and theoretical investigations have been performed. Using mass-analyzed ion kinetic spectrometry, Won *et al.*[17] obtained kinetic energy released distributions (KERD) for different dissociation pathways of CH_3Cl^+ and proposed that CH_3^+ dissociated from $CH_3Cl^+(A^2A_1)$ ion was produced via a direct dissociation whereas the dissociation of $CH_3Cl^+(B^2E)$ ion was statistical. Using complete active space self-consistent-field (CASSCF) and multiconfiguration second-order perturbation theory (CASPT2), Xi *et al.*[18] calculated the Cl-loss and H-loss potential energy curves for

a)Author to whom correspondence should be addressed. Electronic mail: xzhou@ustc.edu.cn.

the lower lying electronic states of CH_3Cl^+, and suggested brief dissociative mechanisms of $CH_3Cl^+(A^2A_1$ and $B^2E)$. In addition, ion-pair dissociation of CH_3Cl was studied by Liu *et al.*[19]

Although many experimental and theoretical studies have been performed on the dissociation of CH_3Cl^+, dissociation mechanism, kinetic energy and internal state distributions of fragments, in addition to the angular distributions of CH_3^+ are still not clarified. Especially, resolution of kinetic energy released during dissociation obtained in Won *et al.*'s experiment[17] is not high enough to determine the vibrational state distribution of CH_3^+, and thereby the detailed information of dissociation dynamics may be buried. In this work, a recently developed TPEPICO velocity map imaging[20] technique has been applied for investigation of dissociation dynamics of state-selected CH_3Cl^+ ions. Due to the high energy resolution of ion velocity imaging,[21–23] velocity distribution of CH_3^+ is measured and its corresponding vibrational distributions are identified. Moreover, angular distributions of CH_3^+ dissociated from specific state-selected CH_3Cl^+ ion are obtained directly from its TPEPICO images as well. Therefore, the overall dissociative mechanism of state-selected $CH_3Cl^+(A^2A_1$ and $B^2E)$ ions will be proposed.

II. EXPERIMENTAL

The present TPEPICO measurements were performed at U14-A beamline of National Synchrotron Radiation Laboratory, Hefei, China. Details of the beamline[24] and the TPEPICO velocity map imaging spectrometer[20] were described previously, and thus only a brief introduction was presented here.

Synchrotron radiation from an undulator was dispersed with a 6 m monochromator equipped with a 370 grooves mm^{-1} spherical grating, and covered the photon energy range of 7.5–22.5 eV. The absolute photon energy scale of the grating was calibrated using the well-known ionization energies of gases, e.g., nitrogen and inert gases (Ar, Kr, and Xe). The resolution power ($E/\Delta E$) of photon energy was about 2000 with 80-μm width entrance and exit slits of the monochromator. A continuous molecular beam (MB) was generated through a 30 μm diameter nozzle with a stagnation pressure of 1.8 atm. The MB intersected with SR at 10 cm downstream after passing through a 0.5-mm diameter skimmer. The typical backing pressures of the source and ionization chambers were 7×10^{-3} Pa and 6×10^{-5} Pa with the MB on.

Photoelectrons and photoions were pushed apart by a dc extraction field, and both of their velocity images were mapped simultaneously at opposite direction. A repelling velocity focusing electric field[20] was utilized to amplify electron image and suppress most part of hot electrons. In addition, a mask with a 1-mm diameter hole and an outside ring located at the end of electron tube was used to collect threshold and hot electrons, and then a subtraction method[25] was employed in threshold photoelectron spectra to eliminate the contamination of hot electrons.

Single-start/multiple-stop[26] data acquisition mode was chosen to record TPEPICO TOF mass spectra of ions, where the measured threshold photoelectrons were used to provide start signals for ions. Through dc electric field of velocity map imaging, ions were accelerated and projected onto a dual micro-channel plate (MCP) backed by a phosphor screen (Burle Industries, P20). To measure TPEPICO velocity images, a high voltage was applied to MCPs as a mass gate, whose duration could be varied from 60 ns to dc depending on the arriving time of target ions. A TE-cooling CCD detector (Andor, DU934N-BV) was used to record the images on the screen. Intensities of the detected electrons and ions were normalized using the photon flux from a silicon photodiode (International Radiation Detectors Inc., SXUV-100).

Commercial CH_3Cl gas (99.9%) without further purification was used in experiments. Due to low photoionization cross section in the excitation energy range of 12–18 eV, a pure CH_3Cl beam was used in measurements of TPES and TPEPICO TOF mass spectra. However, a thermal background in the beam is obvious as shown in the following TOF mass spectra, which will inevitably cause recorded images blurred. Therefore, a CH_3Cl/Ne (1:9) mixture gas was used in our TPEPICO velocity imaging experiments in order to reduce influence of thermal background in the beam.

III. RESULTS AND DISCUSSION

A. Threshold photoelectron spectrum of CH_3Cl in the excitation energy range of 11.0–18.5 eV

With an extraction electric field of 15 V cm^{-1}, TPES of CH_3Cl in the excitation energy range of 11.0–18.5 eV was recorded, where energy increment was 15 meV. As resolution of the present threshold photoelectron energy was about 9 meV (full width at half magnitude, FWHM),[20] main vibrational structures of the electronic states of CH_3Cl^+ could be discerned. Figure 1 shows the modified TPES after subtracting contributions of residual hot electrons.

The lower energy band in Fig. 1 covers an energy range of 11.2–12.2 eV and exhibits a series of resonance peaks,

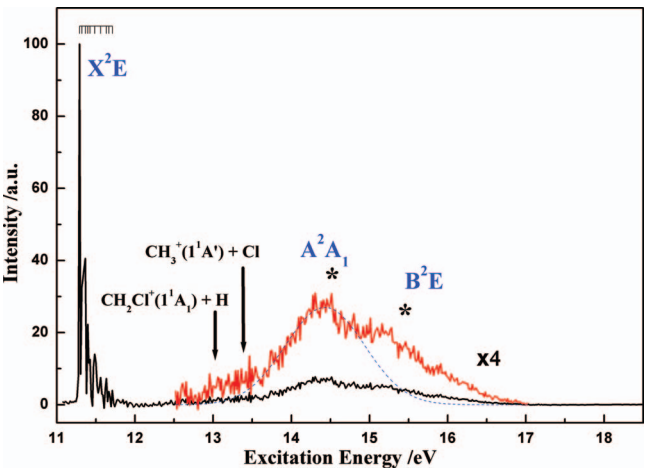

FIG. 1. Threshold photoelectron spectrum of CH_3Cl in the energy range of 11.0–18.5 eV with a step size of 0.015 eV. The energies pointed by arrows are the dissociation limits, and TPEPICO velocity images of CH_3^+ are recorded at the energies noted with stars.

which can be assigned to the vibrational structures of the ground state, $X^2E_{3/2}$ and $X^2E_{1/2}$, of CH_3Cl^+. Both intensities and resonance energies of these vibrational bands agree very well with previous measurements.[1,3] In the energy range of 12.2–18.5 eV, a double-peak band is observed in TPES and no vibrational structure can be discerned, which is very similar to previous TPES (Ref. 1) and high resolution photoelectron spectrum.[3] However, relative intensities of two peaks are much different between the present and previous TPES.[1] In the previous TPES,[1] relative intensity of the double-peak band was close to that of X^2E state, which was quite different with the present observation. It is well known that a major disadvantage in previous TPES measurement is contamination of collected threshold electron by energetic electrons. However, our spectrometer has an excellent ability to suppress hot electrons with application of a decelerating ion lens,[20] and thus the most contaminations of energetic electrons are not involved in TPES. Therefore, the present intensities of all bands in Fig. 1 are believed to be more reliable.

According to the previous spectral assignments,[1,3] both the A^2A_1 and B^2E states of CH_3Cl^+ ions are assigned to the double-peak band, and the intensity of A^2A_1 state is slightly higher than that of B^2E. Due to such a small energy gap between these two excited ionic states, the A^2A_1 and B^2E bands are overlapped in some extent. Thus in the energy range of 14.8–15.6 eV, both the B^2E band and the high-excited vibronic levels of the A^2A_1 state can be excited simultaneously, and hence the corresponding dissociation of CH_3Cl^+ are expected along two dynamic processes from the A^2A_1 state or the B^2E state, which will be discussed in Sec. III F.

B. TPEPICO time-of-flight mass spectra

In the present excitation energy range, many dissociation channels of CH_3Cl^+ ions are possible in thermodynamics, and CH_2Cl^+, CH_3^+, CH_2^+, Cl^+, and HCl^+ fragment ions are expected to be produced. Thus, three TPEPICO TOF mass spectra were measured at photon energies of 11.290, 14.530, and 15.480 eV, respectively, which correspond to the $X^2E_{3/2}$, A^2A_1, and B^2E bands. Only CH_3^+ and CH_2Cl^+ fragment ions were observed among all possible thermodynamic ionic products, and therefore the two most dominant dissociation pathways were investigated in the present work as follows:

$$CH_3Cl^+ \rightarrow CH_2Cl^+(1^1A') + H, \quad (1)$$

$$\rightarrow CH_3Cl^+(1^1A_1) + Cl. \quad (2)$$

In addition, both of them are two lowest channels for dissociation of CH_3Cl^+ ions, and the corresponding dissociation limits are 13.02 eV and 13.38 eV, respectively.[11]

TPEPICO TOF mass spectra measured with an extraction electric field of 15 V cm^{-1} are shown in Fig. 2, where (a) was recorded at 11.290 eV, (b) and (c) were obtained at 14.530 and 15.480 eV, respectively. At 11.290 eV, CH_3Cl^+ ions were generated at the lowest vibronic level of $X^2E_{3/2}$ state. Since the excitation energy was lower than any dissociation limits, only two molecular ions with TOF of 14.55 μs and 14.84 μs were observed, which corresponded to $CH_3{}^{35}Cl^+(m/z = 50)$ and $CH_3{}^{37}Cl^+(m/z = 52)$ ions, respectively. Both isotopes of

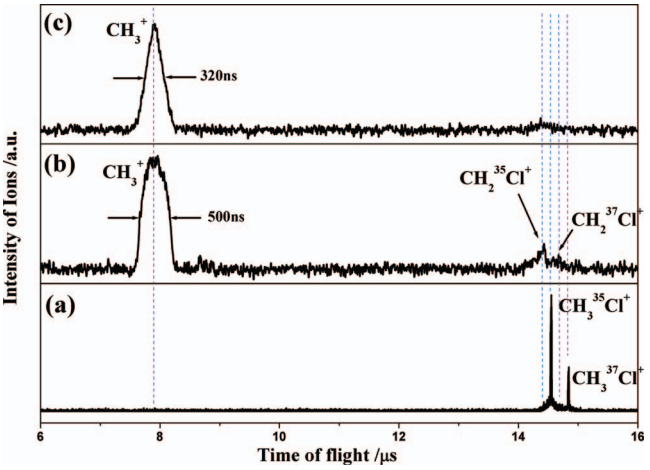

FIG. 2. Energy-selected TPEPICO TOF mass spectra for dissociative photoionization process of CH_3Cl. (a) At 11.290 eV ($X^2E_{3/2}$ state of CH_3Cl^+); (b) at 14.530 eV (A^2A_1); (c) at 15.480 eV (B^2E).

CH_3Cl^+ ion were clearly observed with intensities of their nature abundance. Moreover, the TOF profile of $CH_3{}^{35}Cl^+$ ions showed a wide wing in Fig. 2(a), which was contributed by amounts of thermal background in the beam of pure CH_3Cl gas. Thus, a diluted MB of CH_3Cl/Ne (1:9) was used in order to reduce the thermal background as much as possible during measurement of TPEPICO velocity map imaging.

When the excitation energy was higher than dissociation limits of the channels (1) and (2), both CH_2Cl^+ ($m/z = 49$) and CH_3^+ ($m/z = 15$) fragment ions were clearly observed as shown in Figs. 2(b) and 2(c), while no CH_3Cl^+ ($m/z = 50$, 52) ions existed. Thus, the A^2A_1 and B^2E states of CH_3Cl^+ are unstable and completely dissociative. CH_3^+ fragment ions were kept dominant in the excitation energy range of 13.4–18.5 eV, while the branching ratio of CH_2Cl^+ ions was very low. Compared with the A^2A_1 state, less CH_2Cl^+ ions were produced from $CH_3Cl^+(B^2E)$ ions, which are consistent with the previous results of mass spectra using SR photoionization.[1] However, in the PEPICO investigations using He I light source, no CH_2Cl^+ ions were observed at an excitation energy of lower than 15 eV.[14,15] Similar conclusions were also obtained in photodissociation of CH_3Cl^+ at 366 nm.[16,17] In order to explain the inconsistency, Baer[27] suggested that a dark electronic state of CH_3Cl^+ near A^2A_1 caused C–H bond cleavage, but it was rejected by conclusions of *ab initio* calculation.[18] Only the ground X^2E state adiabatically correlated to the $CH_2Cl^+(1^1A') + H$ dissociation limit among three low-lying electronic states.[18] Therefore, the inconsistency between the present and previous results is believed original from contribution of autoionization process. In SR-based photoionization, molecular ions could be prepared from direct ionization and/or autoionization processes. Thus in the energy range of A^2A_1 state, parts of CH_3Cl^+ ions were also produced at the high vibrational level of X^2E state via autoionization process, and then dissociated to CH_2Cl^+ and H atom along the potential energy surface of X^2E. On the contrary, the autoionization cross section is probably very low at the energy of He I light source, and thus all CH_3Cl^+ ions were generated at the ionic excited electronic state from direct

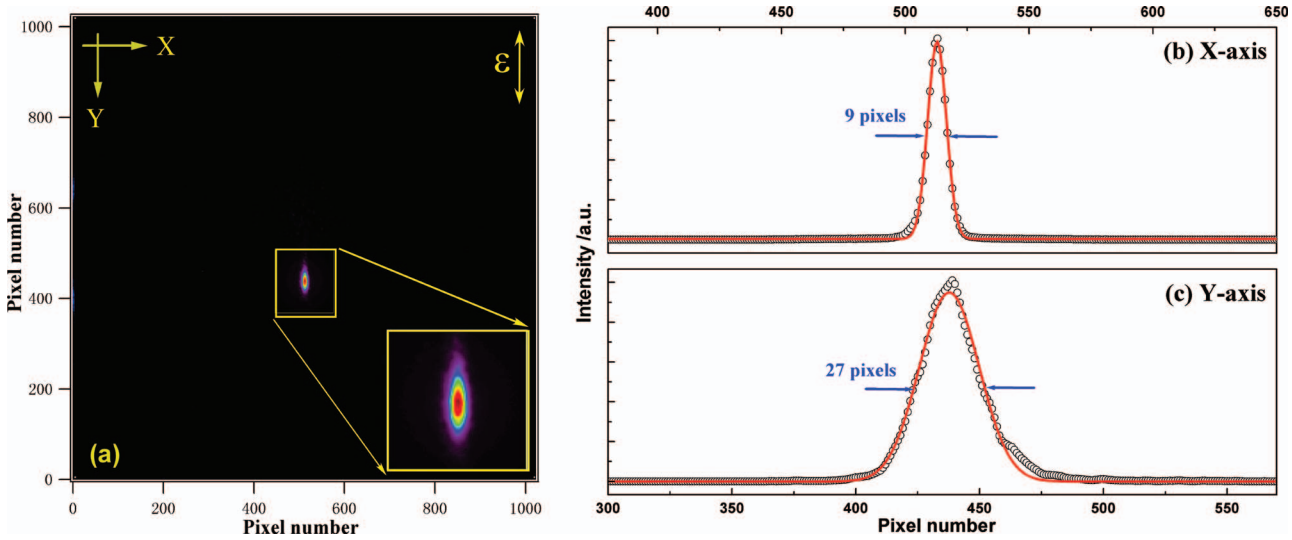

FIG. 3. TPEPICO velocity image and intensity distributions of $CH_3{}^{35}Cl^+(X^2E_{3/2})$ ions at 11.290 eV. (a) The raw image; (b) intensity distributions along x axis, where black circles are experimental data and red line is the least-square fitting with a Gaussian profile; (c) intensity distributions along y axis.

ionization in PEPICO experiments.[14,15] For $CH_3Cl^+(A^2A_1)$ ions, the adiabatic C–H bond cleavage will produce the excited $CH_2Cl^+(^1A'')$ ion and the corresponding dissociation limit is higher than the present excitation energy as calculated in Ref. 18, and hence no CH_2Cl^+ fragments were observed.

As shown in Figs. 2(b) and 2(c), the widths of two TOF peaks of CH_2Cl^+ and $CH_3{}^+$ were broadened due to released kinetic energy in dissociation. As the signal-to-noise ratio of CH_2Cl^+ fragment ion was poor, we did not measure its TPEPICO velocity image. For $CH_3{}^+$ fragment ion, its TOF profile in Fig. 2(b) was recorded with a nearly rectangular contour and a FWHM of 500 ns at 14.530 eV, implying that dissociation along the channel (2) is fast. It was very interesting that the TOF profile of $CH_3{}^+$ changed its contour to a nearly triangle when the excitation energy was increased to 15.480 eV, as shown in Fig. 2(c). Moreover, its FWHM decreased to 320 ns although the available energy for the dissociation channel (2) was increased much. Since $CH_3Cl^+(A^2A_1)$ and $CH_3Cl^+(B^2E)$ ions were mostly prepared at 14.530 eV and 15.480 eV, respectively, dissociative mechanisms of CH_3Cl^+ ions along the channel (2) are expected to be entirely different for the A^2A_1 and B^2E states.

C. TPEPICO velocity image of CH_3Cl^+ in the $X^2E_{3/2}$ state

Kinetic energy resolution of the present ion velocity imaging is better than 3% of $\Delta E/E$,[20] and hence vibrational state population of fragment can be discerned. Therefore, we performed TPEPICO velocity imaging measurements for the X^2E, A^2A_1, and B^2E electronic states of CH_3Cl^+ ions, respectively.

At 11.290 eV, no fragmentation process of CH_3Cl^+ happened. Thus, only image of $CH_3{}^{35}Cl^+$ ions was recorded and presented in Fig. 3(a), where SR propagated along the direction of x axis, and electric vector ε of photon was along y axis. Since MB flew along y axis from top to bottom and the TOF axis was perpendicular to MB, the image of $CH_3{}^{35}Cl^+$ ions was eccentric from the center of CCD along the beam direction as shown in Fig. 3(a).

Due to a perpendicular geometry of MB direction and the TOF axis, the velocity spread of beam inevitably causes recorded images broadened along MB direction (y axis).[20,21,28] On the contrary, the image along x axis is scarcely affected due to collimation of the skimmer. As Figs. 3(b) and 3(c) shown, intensity distributions of the image along x axis and y axis have Gaussian profiles, where the FWHMs are 9 and 27 pixels, respectively. Thus, the recorded image presents an elliptical contour in Fig. 3(a). In this case, the real ion images need to be handled prior to extracting speed and angular distributions through a multi-step data reduction scheme including quadrant symmetrization and deconvolution. Its details have been described in the supplementary material of Ref. 28. From the intensity distribution in Fig. 3(c), the parallel translational temperature of MB can be estimated as 18 K,[29] which will be used in deconvolution of $CH_3{}^+$ images in Secs. III D–III E.

D. TPEPICO 3D time-sliced velocity image of $CH_3{}^+$ in the A^2A_1 state

Figure 4(a) shows the recorded TPEPICO 3D time-sliced image of $CH_3{}^+$ dissociated from $CH_3Cl^+(A^2A_1)$ ions at 14.530 eV, where a mass gate of 60 ns was applied. Besides a major structure of multi-ring, there is a bright off-centered spot, which is composed by CH_3Cl^+ ions from false coincidence events. The pure image of $CH_3{}^+$ fragment can be obtained through subtracting a false coincidence image as described in Ref. 30. Subsequently, the data reduction process of deconvolution and quadrant symmetrization is necessary to obtain the real ion images, in order to subtract contamination in the raw images from velocity spread of MB. Thus the modified image of $CH_3{}^+$ fragment ions at 14.530 eV is presented in Fig. 4(b), where the direction of MB and electric vector ε of photon are fixed as the same as Fig. 3(a).

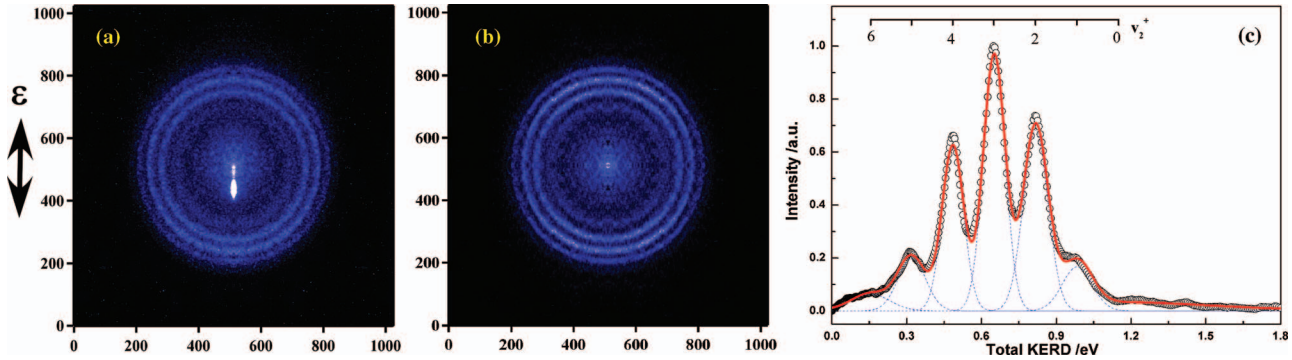

FIG. 4. TPEPICO 3D time-sliced images of CH_3^+ ions and total kinetic energy released distributions from dissociation of $CH_3Cl^+(A^2A_1)$ ions at 14.530 eV. (a) The raw image; (b) the modified image; (c) the corresponding total kinetic energy released distributions, where circles are experimental data and the least-square fitting with six Gaussian profiles are shown with solid line.

A series of homocentric rings are clearly observed in Fig. 4(b), which is contributed by CH_3^+ ions with different velocities. By accumulating intensity of the image over angles, speed distribution of CH_3^+ fragment ions is acquired directly. From the conservation of linear momentum, total KERD in dissociation of $CH_3Cl^+(A^2A_1)$ ions can be obtained and shown in Fig. 4(c). Benefit from high energy resolution of velocity imaging, the present KERD shows more clear internal energy distributions than previous results,[15,17] that five distinct peaks corresponding to vibrational excitation of fragment are observed in the total KERD. Based on the energy conservation in dissociation, assignment of these peaks in terms of the vibrational states of CH_3^+ can be obtained and shown in Fig. 4(c). Relation between the internal energy of CH_3^+ fragment ion, E_{int}, and the total released kinetic energy, E_T, can be expressed as the following formula:

$$h\upsilon - D_0 = E_{avail} = E_{int} + E_T, \tag{3}$$

where $h\upsilon$ is photon energy, E_{avail} is available energy after dissociation and D_0 is the dissociation limit for a specific channel.

In the dissociation process to form CH_3^+, the C–Cl bond of CH_3Cl^+ ions is broken and carbon atom moves towards the plane of three H atoms under the action of the recoil momentum of the leaving chloride atom. As such a movement is very similar to the umbrella vibration (v_2^+) of CH_3^+, the v_2^+ mode is expected to be dominantly excited during the fast dissociation. In fact, the energy intervals between the adjacent peaks in Fig. 4(c) are very close to the $v_2^+(CH_3^+)$ vibrational frequency, 1380 cm^{-1}.[19,31] Taking the dissociation limit $D_0 = 13.38$ eV for the $CH_3^+(1^1A_1) + Cl$ channel,[11] the maximal v_2^+ quantum number of CH_3^+ is equal to 6. Therefore, the possible vibrational state population of CH_3^+ dissociated from $CH_3Cl^+(A^2A_1)$ ions can be assigned and shown in Fig. 4(c) as well. Moreover, relative intensities of every vibrational state can be estimated through fitting the total KERD with six Gaussian profiles, and summarized in Table I. Obviously, an occurrence of vibrational population reversion is happened for $CH_3^+(1^1A_1)$ fragment ions. As the assignments shown, the maximum vibrational population of $CH_3^+(1^1A_1)$ is located at $v_2^+ = 3$. In addition, no other vibration modes of CH_3^+ are observed in the total KERD, indicating that the C_{3V} geometry of CH_3^+ moiety is kept during dissociation and no distinct intermolecular vibrational redistribution happens.

From the image of Fig. 4(b), angular distributions of CH_3^+ fragment ions can be derived by integrating the image over a proper range of speed at each angle. Consequently, anisotropic parameters β for dissociation pathways to form $CH_3^+(1^1A_1)$ in a special vibrational state can be calculated by fitting the angular distribution, $I(\theta)$, with the following formula:[32]

$$I(\theta) = \frac{1}{4\pi}\left[1 + \beta \cdot P_2(\cos\theta)\right], \tag{4}$$

where θ is the angle between the recoil velocity of fragment and the electric field vector ε of photon, and $P_2(\cos\theta)$ is the second-order Legendre polynomial. Thus the anisotropic parameters β for $CH_3^+(1^1A_1)$ ions in the vibrational states of $v_2^+ = 2$, 3, and 4 are obtained to be 0.44, 0.37, and 0.22, which are listed in Table I as well. For $CH_3^+(1^1A_1)$ at the other vibrational states, e.g., $v_2^+ = 1$ and 5, the β values are estimated to be 0.5 and 0.1, respectively, but relative large uncertainties exist due to their poor signal-to-noise ratios in images. Thus we do not summarize them in Table I. Obviously, all β values are positive, indicating that dissociation of $CH_3Cl^+(A^2A_1)$ ions has a character of parallel transition. In addition, a dependence of β on the vibrational states of $CH_3^+(1^1A_1)$ ions is shown, which will be discussed in Sec. III F.

TABLE I. Vibrational state distribution of CH_3^+ dissociated from CH_3Cl^+ ions at 14.530 eV.

Vibronic level of $CH_3^+(1^1A_1)$	Relative intensity	FWHM of profile (eV)	Anisotropic *parameter, β*
$v_2^+ = 0$	< 0.01	...	...
$v_2^+ = 1$	0.17	0.09	...
$v_2^+ = 2$	0.72	0.07	0.44 ± 0.09
$v_2^+ = 3$	1.00	0.06	0.37 ± 0.07
$v_2^+ = 4$	0.64	0.06	0.22 ± 0.09
$v_2^+ = 5$	0.21	0.08	...
$v_2^+ = 6$	0.07	0.11	...

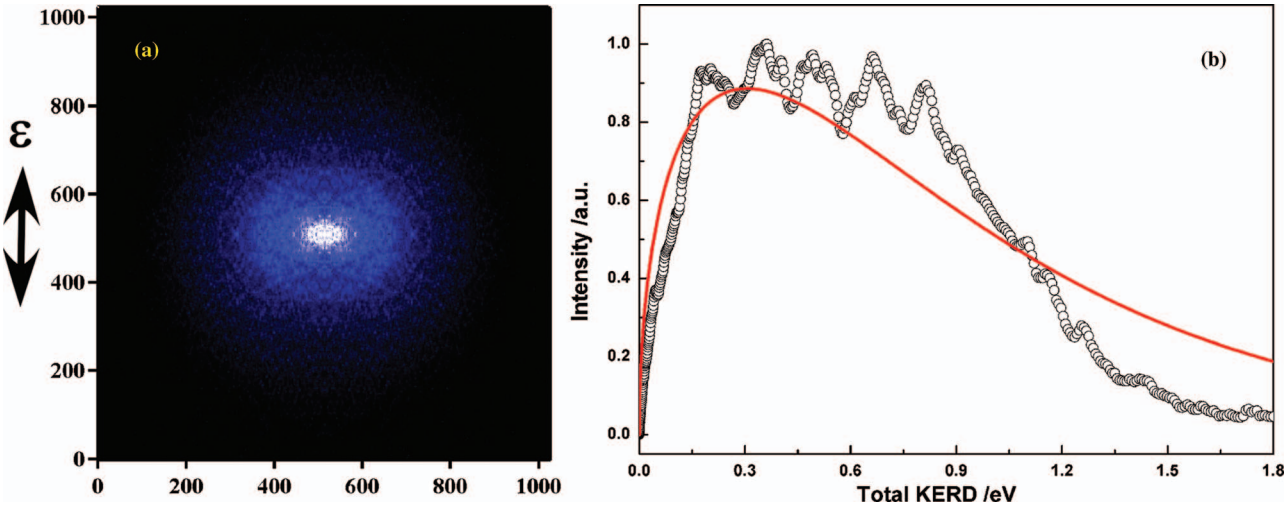

FIG. 5. TPEPICO 3D time-sliced images of CH_3^+ ions and total kinetic energy released distributions from dissociation of $CH_3Cl^+(B^2E)$ ions at 15.480 eV. (a) The modified image; (b) the corresponding total kinetic energy released distributions, where circles are experimental data and the least-squares fitting with a Maxwell-Boltzmann profile are shown with solid line.

E. TPEPICO 3D time-sliced velocity image of CH_3^+ in the B^2E state

Fixed photon energy at 15.480 eV, $CH_3Cl^+(B^2E)$ ions were mainly generated and subsequently dissociated. The modified TPEPICO 3D time-sliced image of CH_3^+ fragment ions was shown in Fig. 5(a). Different from the structure of homocentric rings in Fig. 4(b), only a pancake was observed in Fig. 5(a), where the brightest part was located at the center.

Through the data reduction process of substraction, deconvolution, and quadrant symmetrization as described in Ref. 28, total KERD in dissociation of CH_3Cl^+ ions at 15.480 eV was obtained and presented in Fig. 5(b). The average released kinetic energy in dissociation is obviously smaller than that of $CH_3Cl^+(A^2A_1)$ ions, which is consistent with that suggested by the FWHM of TOF profiles in Fig. 2. Moreover, the total KERD curve shows a near Maxwell-Boltzmann profile as the red line in Fig. 5(b), indicating that the CH_3^+ formation pathway of $CH_3Cl^+(B^2E)$ ions is slow via a statistical dissociation. These speculations were also suggested by previous experimental studies.[15]

Interestingly, several peaks superimpose over a broadened background in the total KERD curve of Fig. 5(b), and energy intervals between these peaks look very close to those in Fig. 4(c). Thus the umbrella vibration (v_2^+) of CH_3^+ seems to be prominently excited during dissociation, which is inconsistent with the statistical dissociation of $CH_3Cl^+(B^2E)$ ions. However, as shown in TPES of Fig. 1, CH_3Cl^+ ions can be prepared in both the B^2E state and the high-excited vibronic levels of the A^2A_1 state at 15.480 eV, although the most part of CH_3Cl^+ ions were certainly in the B^2E state. Therefore, dissociation from the minority CH_3Cl^+ ions at the high-excited vibronic levels of A^2A_1 contributes the peaks in total KERD curve of Fig. 5(b).

From the image of Fig. 5(a), the angular distribution of CH_3^+ was plotted as shown in Fig. 6. The angular distributions were very similar for all released kinetic energies. Using the formula (4), the anisotropic parameter β is obtained to be -0.32. Therefore, dissociation of $CH_3Cl^+(B^2E)$ has a character of perpendicular transition and is entirely different from the parallel dissociation of $CH_3Cl^+(A^2A_1)$.

F. Dissociative mechanism of CH_3Cl^+ ions

From the images and total KERD curves in Figs. 4 and 5, the energy distributions of CH_3^+ dissociated from CH_3Cl^+ ions at 14.530 and 15.480 eV can be estimated. The average total released kinetic energies, $\langle E_T \rangle$, as well as the average vibrational energy $\langle E_{vib} \rangle$ and rotational energy $\langle E_{rot} \rangle$ of CH_3^+, are summarized in Table II.

In the A^2A_1 state, CH_3Cl^+ dissociates fast along the C–Cl bond rupture with C_{3V} geometry. "Impulsive model" is expected to describe its dissociative mechanism, in which the proportion of average total kinetic energy $\langle E_T \rangle$ and available energy E_{avail} can be calculated as the following formula:

$$f_T = \frac{\langle E_T \rangle}{E_{avail}} = \frac{\mu_{C-Cl}}{\mu_{CH_3-Cl}} = 0.85, \quad (5)$$

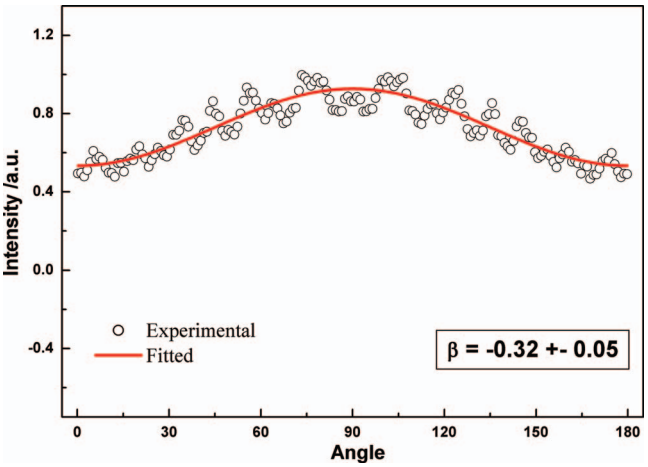

FIG. 6. Experimental and fitted angular distributions of CH_3^+ dissociated from $CH_3Cl^+(B^2E)$ at 15.480 eV, where open circles represent experimental data and solid line is the fitted curve.

TABLE II. Energy distribution of CH_3^+ dissociated from CH_3Cl^+ ions.

$h\nu$ (eV)	E_{avail} (eV)	$\langle E_T\rangle$ (eV)[a]	$f_T = \langle E_T\rangle/E_{avail}$	$\langle E_{vib}\rangle$ (eV)[b]	$\langle E_{rot}\rangle$ (eV)[c]
A^2A_1					
14.530	1.15	0.612	0.532	0.52	0.02
B_2E					
15.480	2.20	0.508	0.231		

[a] $\langle E_T\rangle$ is the average total kinetic energy released in dissociation.
[b] $\langle E_{vib}\rangle$ is the average vibrational energy of CH_3^+.
[c] $\langle E_{rot}\rangle$ is the average rotational energy of CH_3^+, $\langle E_{rot}\rangle = \langle E_{avail}\rangle - \langle E_T\rangle - \langle E_{vib}\rangle$.

where μ is reduced mass. In this case, the geometry of methyl group is initially kept during the fast dissociation until separation of Cl atom and CH_3. The final umbrella vibration energy of CH_3 will be distributed from its initial kinetic energy. However, only 53% of available energy is taken by the translation of CH_3^+ ion and Cl atom at 14.530 eV as shown in Table II. Therefore, the partial relaxation of methyl group happens to change from the tetrahedral structure to planar during the impulsive period of the dissociation process.

As shown in Table I, a dependence of β on the vibrational states of $CH_3^+(1^1A_1)$ is observed, which does not agree with a usual conclusion of fast dissociation along a repulsive potential energy surface. Thus, details of potential energy surface of $CH_3Cl^+(A^2A_1)$ need to be carefully examined. The Cl-loss potential energy curves of the low-lying electronic states of CH_3Cl^+ are shown in Fig. 7, which are obtained by plotting the calculated energies of electronic states at different C–Cl bond length in Table III of Ref. 18. As the slight energy shifts exist between experimental and calculated dissociation limits, we vertically shifted the calculated curves in Fig. 7 in order to match the experimental dissociation limits. It needs to be noted that the X^2E and B^2E states should be divided to $^2A'$ and $^2A''$ states when taking into account Jahn-Teller distortion, however, only a little difference was observed between the Cl-loss potential energy curves of the $^2A'$ and $^2A''$ states.[18] Therefore, we did not involve this effect in discussing the dissociative mechanism of CH_3Cl^+ ions, as shown in Fig. 7.

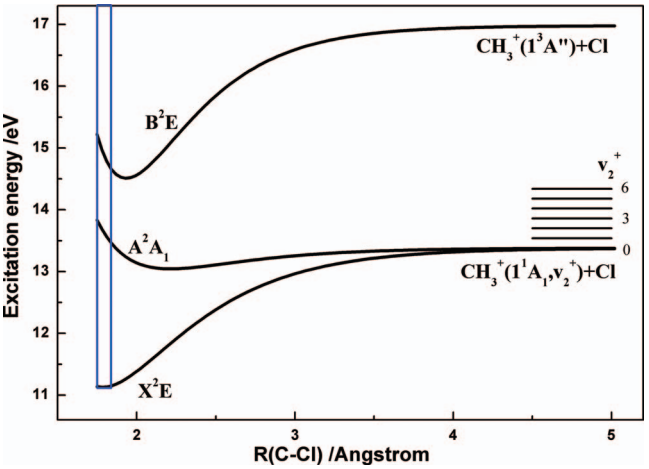

FIG. 7. The Cl-loss potential energy curves of the low-lying electronic states of CH_3Cl^+ ion along the C–Cl bond length, where the calculated curves from Ref. 18 are slightly vertically shifted to match the experimental dissociation limits. The Frank-Condon area is shown with blue pane.

For the A^2A_1 state, it adiabatically correlates to the $CH_3^+(1^1A_1)$ + Cl dissociation limit. In the Frank-Condon area, the steep repulsive potential initially pushes Cl atom far away quickly, and methyl group is almost kept the original tetrahedral geometry. However, a shallow potential well exists along the C–Cl bond rupture as shown in Fig. 7, although it is not a true minimum in the CASSCF full geometry optimization calculation.[18] Thus, the binding interaction of the potential well is stronger with the v_2^+ quantum number increasing, and hence the dissociation time scale of $CH_3Cl^+(A^2A_1)$ to produce the $CH_3^+(1^1A_1,v_2^+)$ fragment ion is expected increasing. Consequently, the CH_3^+ formation process from $CH_3Cl^+(A^2A_1)$ ions tends to be isotropic as the v_2^+ quantum number increases.

As shown in Fig. 7, the B^2E state is typical bound and adiabatically correlates to the $1^3A''$ excited electronic state of CH_3^+. Because the present excitation energy is lower than the adiabatically dissociation limit, the probable C–Cl cleavage of $CH_3Cl^+(B^2E)$ ions is through internal conversions to the lower electronic states, A^2A_1 or X^2E. According to the perpendicular dissociation of $CH_3Cl^+(B^2E)$ with the β value of −0.32, the unique potential mechanism is via internal conversion to the high vibrational state of X^2E and subsequently statistical dissociation.

IV. CONCLUSIONS

Using synchrotron radiation as light source and TPEPICO velocity imaging, state-selected dissociation dynamics of CH_3Cl^+ ions were investigated. In the excitation energy range of 11.0–18.5 eV, the X^2E, A^2A_1, and B^2E states of CH_3Cl^+ were observed in threshold photoelectron spectrum. The A^2A_1 and B^2E bands show diffuse structures and partially overlapped, indicating that both of them are fully dissociative (or predissociative).

The energy-selected TPEPICO TOF mass spectra were recorded for the photoionization processes of CH_3Cl at 11.290, 14.530, and 15.480 eV, respectively, where CH_3Cl^+, CH_3^+, and CH_2Cl^+ fragment ions were clearly observed. CH_3^+ was kept as the most dominant fragment ions in the present excitation energy range while the branching ratio of CH_2Cl^+ ions was very low. According to the inconsistency of experimental results between the present and previous PEPICO studies, CH_2Cl^+ fragment ions observed at the excitation energy range of $CH_3Cl^+(A^2A_1)$ are believed original from dissociation of high vibronic level of $CH_3Cl^+(X^2E)$ produced in autoionization process.

In order to reveal the CH_3^+ formation pathway, 3D time-sliced TPEPICO velocity map images of CH_3^+ dissociated from $CH_3Cl^+(A^2A_1$ and $B^2E)$ ions were recorded. KERD and angular distribution were obtained subsequently from the images. For the A^2A_1 state, a series of homocentric rings is clearly observed and assigned as the excitation of umbrella vibration of CH_3^+ during dissociation. Thus, the CH_3^+ moiety is kept with C_{3V} geometry during dissociation as no other vibrational modes are observed in the total KERD. Moreover, the obtained β values are positive, indicating that dissociation of $CH_3Cl^+(A^2A_1)$ ions has a character of parallel transition. In addition, a dependence of β on the vibrational states of

$CH_3^+(1^1A_1)$ ions is clearly observed, which provides a direct experimental evidence of a shallow potential well along the C–Cl bond rupture.

Different from the rapid dissociation, the total KERD of CH_3^+ fragmentation from $CH_3Cl^+(B^2E)$ ions did exhibit a near Maxwell-Boltzmann profile. Besides $CH_3Cl^+(B^2E)$ ions, the minority CH_3Cl^+ ions at the high-excited vibronic levels of the A^2A_1 state were simultaneously produced at 15.480 eV, which contributed the small peaks superimposed over a broadened background in the total KERD curve.

With the aid of previous calculated potential energy curves of CH_3Cl^+ along the C–Cl ruptures, the dissociative mechanisms of CH_3Cl^+ in the A^2A_1 and B^2E states are obtained. $CH_3^+(A^1A')$ fragment ions can be produced from $CH_3Cl^+(A^2A_1)$ via a rapid direct dissociation, while $CH_3Cl^+(B^2E)$ ions can dissociate via internal conversion to the high vibrational states of X^2E and subsequently statistical dissociation.

ACKNOWLEDGMENTS

Financial supports from the National Natural Science Foundation of China (NSFC, (Nos. 10979042 and 21073173) and National Key Basic Research Special Foundation (NKBRSF, Nos. 2007CB815204 and 2010CB923300) are appreciated. X. Zhou also thanks the Fundamental Research Funds for the Central Universities (No. WK2060030006) and USTC-NSRL Association funding (No. KY2060030007) for supports.

[1]R. Locht, B. Leyh, A. Hoxha, D. Dehareng, K. Hottmann, H. W. Jochims, and H. Baumgartel, Chem. Phys. **272**, 293 (2001).
[2]T. N. Olney, G. Cooper, W. F. Chan, G. R. Burton, C. E. Brion, and K. H. Tan, Chem. Phys. **205**, 421 (1996).
[3]L. Karlsson, R. Jadrny, L. Mattsson, F. T. Chau, and K. Siegbahn, Phys. Scr. **16**, 225 (1977).
[4]R. Locht, B. Leyh, A. Hoxha, D. Dehareng, H. W. Jochims, and H. Baumgartel, Chem. Phys. **272**, 277 (2001).
[5]D. M. P. Holland, I. Powis, G. Ohrwall, L. Karlsson, and W. von Niessen, Chem. Phys. **326**, 535 (2006).
[6]I. Novak, J. M. Benson, and A. W. Potts, J. Electron. Spectrosc. Relat. Phenom. **41**, 225 (1986).
[7]Y. Hikosaka, J. H. D. Eland, T. M. Watson, and I. Powis, J. Chem. Phys. **115**, 4593 (2001).
[8]S. Tsuda and W. H. Hamill, J. Chem. Phys. **41**, 2713 (1964).
[9]S. Tsuda, C. E. Melton, and W. H. Hamill, J. Chem. Phys. **41**, 689 (1964).
[10]F. P. Lossing, Bull. Soc. Chim. Belg. **81**, 125 (1972).
[11]A. S. Werner, B. P. Tsai, and T. Baer, J. Chem. Phys. **60**, 3650 (1974).
[12]B. Brunetti, P. Candori, J. DeAndres, F. Pirani, M. Rosi, S. Falcinelli, and F. Vecchiocattivi, J. Phys. Chem. A **101**, 7505 (1997).
[13]M. Alberti, J. M. Lucas, B. Brunetti, F. Pirani, M. Stramaccia, M. Rosi, and F. Vecchiocattivi, J. Phys. Chem. A **104**, 1405 (2000).
[14]J. H. D. Eland, R. Frey, A. Kuestler, H. Schulte, and B. Brehm, Int. J. Mass Spectrom. Ion Process. **22**, 155 (1976).
[15]I. C. Lane and I. Powis, J. Phys. Chem. **97**, 5803 (1993).
[16]R. G. Orth, and R. C. Dunbar, J. Chem. Phys. **68**, 3254 (1978).
[17]D. S. Won, M. S. Kim, J. C. Choe, and T. K. Ha, J. Chem. Phys. **115**, 5454 (2001).
[18]H. W. Xi, M. B. Huang, B. Z. Chen, and W. Z. Li, J. Phys. Chem. A **109**, 4381 (2005).
[19]X. H. Liu, R. L. Gross, and A. G. Suits, Science **294**, 2527 (2001).
[20]X. F. Tang, X. G. Zhou, M. L. Niu, S. L. Liu, J. D. Sun, X. B. Shan, F. Y. Liu, and L. S. Sheng, Rev. Sci. Instrum. **80**, 113101 (2009).
[21]A. Eppink and D. H. Parker, Rev. Sci. Instrum. **68**, 3477 (1997).
[22]H. F. Xu, Y. Guo, Q. F. Li, Y. Shi, S. L. Liu, and X. X. Ma, J. Chem. Phys. **121**, 3069 (2004).
[23]H. Wang, X. G. Zhou, S. L. Liu, B. Jiang, D. X. Dai, and X. M. Yang, J. Chem. Phys. **132**, 244309 (2010).
[24]S. S. Wang, R. H. Kong, X. B. Shan, Y. W. Zhang, L. S. Sheng, Z. Y. Wang, L. Q. Hao, and S. K. Zhou, J. Synchrotron Radiat. **13**, 415 (2006).
[25]B. Sztaray and T. Baer, Rev. Sci. Instrum. **74**, 3763 (2003).
[26]A. Bodi, B. Sztaray, T. Baer, M. Johnson, and T. Gerber, Rev. Sci. Instrum. **78**, 084102 (2007).
[27]T. Baer, A. S. Werner, B. P. Tsai, and S. F. Lin, J. Chem. Phys. **61**, 5468 (1974).
[28]X. F. Tang, M. L. Niu, X. G. Zhou, S. L. Liu, F. Y. Liu, X. B. Shan, and L. S. Sheng, J. Chem. Phys. **134**, 054312 (2011).
[29]D. Irimia, R. Kortekaas, and M. H. M. Janssen, Phys. Chem. Chem. Phys. **11**, 3958 (2009).
[30]X. F. Tang, X. G. Zhou, M. L. Niu, S. L. Liu, and L. S. Sheng, J. Phys. Chem. A **115**, 6339 (2011).
[31]M. E. Jacox, J. Phys. Chem. Ref. Data **27**, 213 (1998).
[32]R. N. Zare, Mol. Photochem. **4**, 1 (1972).